Title

High Contrast Reflectance Imaging of Enamel Demineralization and Remineralization at 1950-nm for the Assessment of Lesion Activity

Journal

Lasers in Surgery and Medicine, 53(7)

ISSN

0196-8092

Authors

Fried, William A
Abdelaziz, Marwa
Darling, Cynthia L
et al.

Publication Date

2021-09-01

DOI

10.1002/lsm.23371

Peer reviewed

HHS Public Access

Author manuscript

Lasers Surg Med. Author manuscript; available in PMC 2022 September 01.

Published in final edited form as:

Lasers Surg Med. 2021 September ; 53(7): 968–977. doi:10.1002/lsm.23371.

High Contrast Reflectance Imaging of Enamel Demineralization and Remineralization at 1950-nm for the Assessment of Lesion Activity

William A. Fried, **Marwa Abdelaziz, DDS, PhD**, **Cynthia L. Darling, PhD**, **Daniel Fried, PhD**[α]

Department of Preventive and Restorative Dental Sciences, University of California San Francisco, CA 94143

Abstract

Objective: Previous studies have shown that large changes in the diffuse reflectivity of caries lesions during drying with air can be used to assess lesion activity. The largest changes occur at short wavelength infrared (SWIR) wavelengths coincident with high water absorption. The strongest water absorption in the SWIR occurs at 1950-nm. In this study changes in the reflectivity of simulated lesions with varying degrees of remineralization was measured at 1500–2340-nm and at 1950-nm as the samples were dried with air.

Methods: Twenty bovine enamel surfaces each with 5 treatment windows were exposed to two demineralization/remineralization regimens to produce simulated lesions of varying depth, severity and mineral gradients. An extended range tungsten-halogen lamp with a long pass filter (1500–2340-nm) and a broadband ASE source centered near the peak of the water-absorption band at 1950-nm were used as light sources and an extended range InGaAs camera (1000–2340-nm) was used to acquire reflected light images as the samples were dried with air. Lesions were also assessed using digital microscopy, polarized light microscopy (PLM), optical coherence tomography (OCT), and transverse microradiography (TMR).

Results: Both wavelength ranges showed extremely high lesion contrast (> 0.9) for all six lesion treatment windows in both models. The change in contrast (ΔI) was significantly higher for the 1950-nm broadband source for all the intact lesion windows compared to the 1500–2340-nm wavelength range.

Conclusion: SWIR light at 1950-nm yields extremely high contrast of demineralization and appears to be the optimum wavelength for the assessment of lesion activity on tooth coronal surfaces.

Keywords

dental caries; lesion activity; SWIR Imaging; enamel; lesion dehydration

[α]To whom correspondence should be addressed: Daniel Fried, Ph.D., Department of Preventive and Restorative Dental Sciences, 707 Parnassus Avenue, University of California San Francisco, CA 94143-0758, Daniel.fried@ucsf.edu.

INTRODUCTION

The nature of dental decay or caries in the U.S. has changed markedly due to the introduction of fluoride to the drinking water, the use of fluoride dentifrices and rinses, and improved dental hygiene. Despite these advances, dental caries continues to be the leading cause of tooth loss in the U.S. [1–3]. Tooth structure undergoes demineralization from organic acids produced by bacteria plaque forming active caries lesions [1]. Such lesions can also undergo remineralization that can reverse the caries process by repairing existing crystal remnants with the help of calcium and phosphate ions, primarily from saliva, and fluoride ions from topical sources thereby arresting the lesion. Fluoride inhibits demineralization and enhances remineralization by promoting crystal growth and producing fluorapatite crystals that are much more resistant to an acid challenge than the pure phase hydroxyapatite of enamel and dentin.

Therefore, caries lesions can be either active requiring further intervention or inactive or arrested requiring no further treatment [2]. Unfortunately, reliable methods for the assessment of lesion activity are lacking and current methods rely on visual and tactile assessment that are highly subjective. Visual assessment relies on color and texture which lacks specificity and tactile assessment with a dental explorer may harm arrested lesions accelerating further decay [2]. The International Caries Detection and Assessment System (ICDAS) II criteria for enamel caries lesion activity assessment was introduced in an attempt to standardize visual assessment [2–5]. However, this approach still relies on visual assessment and has the same limitations.

Histopathology of enamel caries in the old and young has shown that lesions in old permanent teeth had thicker and more distinct surfaces zones than those on more recent lesions on younger teeth [6]. *In vivo* studies of lesion arrest after the removal of orthodontic bands showed that remineralization produced hard shiny lesions with some remaining interior subsurface demineralization and that the well-mineralized surface layer forms a diffusion barrier against the subsurface uptake of minerals from saliva [7–9]. Mineral deposition during remineralization typically occurs first in the outer most layers of the lesion producing a highly mineralized surface zone or “scab” that inhibits further diffusion of fluids into the lesion effectively arresting further lesion progression [6]. Therefore, the presence of a highly mineralized surface zone covering the lesion is a key indicator that the lesion is arrested. Histological methods such as transverse microradiography (TMR) and polarized light microscopy (PLM) can be used to detect this lesion surface zone however such methods require destruction of the tooth and are unsuitable for use *in-vivo* [10–12]. If the mineral content of that outer surface zone is high enough it has increased transparency allowing the surface layer to be detected and measured using optical coherence tomography (OCT) and several studies both *in vitro* and *in vivo* have shown that OCT can be used to detect this transparent surface zone [13–17]. In addition, methods have been developed to automatically detect the transparent surface layer of enamel lesions exposed to remineralization solutions and measure its thickness [17].

As the lesion becomes arrested by mineral deposition or remineralization, the permeability of the mineralized surface layer decreases. Thus, the rate of diffusion of water from the

lesion is greatly reduced if the lesion is arrested. Changes in fluorescence loss [18–20], thermal emission and SWIR reflectance [21–23] during lesion dehydration have been investigated as methods for assessing lesion activity. *In-vivo* studies have been published utilizing the fluorescence loss of white spot lesions on coronal surfaces [20] and thermal imaging to assess root caries during dehydration [24]. The relationship between surface zone thickness and lesion permeability is highly non-linear; a small increase in the surface layer thickness can lead to a marked decrease in permeability [25].

SWIR reflectance imaging has also been exploited for caries detection because sound enamel is transparent in the SWIR and the scattering coefficient increases significantly with increasing mineral loss [26–33]. Zakian et al. [34] carried out SWIR reflectance measurements from 1000 – 2500 nm using a hyperspectral imaging system and showed that the reflectance from sound tooth structure decreases at longer wavelengths where water absorption is higher. Further measurements over the past ten years have shown that the contrast between sound and demineralized enamel continues to increase with increasing wavelength [28,30] due to the decreasing scattering coefficient of sound enamel [27], increased water absorption and decreased interference from stains [29]. The maximum attainable contrast between sound and demineralized enamel, and the degree of change in contrast with the depth and severity of demineralization depends on the wavelength [31,35]. Therefore, it is important to measure lesions of varying depth, degree of demineralization and mineral gradient when comparing lesion contrast at different wavelengths.

Few studies have looked at the contrast of caries lesions at wavelengths beyond 1700-nm due to the limited sensitivity range of conventional InGaAs sensors and the limited availability of high intensity broadband light sources in this range. In this study, two devices that have just recently become available, were used to image lesions near the strong water absorption band at 1950-nm. A broadband, high power ASE source centered near the peak of the water-absorption band at 1950-nm and an extended range InGaAs camera (1000–2340-nm) were used to acquire reflected light images of simulated lesions of varying degree of demineralization and remineralization as they were dried with air at 1950-nm.

MATERIALS AND METHODS

2.1 Sample Block Preparation

Two sets of samples each with ten blocks were prepared for this study from extracted bovine incisors acquired from a slaughterhouse. Flattened bovine enamel blocks are a suitable substitute for human enamel in the study of dental caries and yield more uniform lesions upon demineralization [36]. Each block was approximately 10–14 mm in length with a width of 3 mm and a thickness of 2 mm. Extra blocks were prepared for analysis by polarized light microsopy (PLM) and transverse microradiography (TMR). Each sample was partitioned into 5 or 6 windows by etching small incisions 2.5 mm apart across each of the blocks using a laser as can be seen in Figs. 2 & 3. Incisions were etched using a radio-frequency (RF) excited industrial CO_2 laser, a Coherent Diamond J-5V Series (Coherent Inc., Santa Clara, CA), operating at 9.4 μm with a pulse duration of 25 μs and a pulse repetition rate of 100 Hz.

A surface softened lesion model, that produces subsurface demineralization without erosion of the surface [37] was used to create lesions on the central three windows on all 20 bovine blocks. The mineral loss profiles are fairly uniform in these lesions and they emulate an active lesion. The lesions produced were approximately 80–100-μm deep. Each set of bovine blocks was subsequently exposed to a different remineralization regimen to produce lesions of varying mineral gradients. The first set of ten blocks was exposed to a neutral remineralization solution and the second set was exposed to an acidic remineralization solution. There were five windows on each of the samples, sound untreated (S), lesion only (L), lesion exposed to 4-days of remineralization (4D), lesion exposed to 12-days of remineralization (12D), and sound window exposed to 12-days of remineralization (R) which served as a control. A thin layer of acid-resistant varnish in the form of nail polish, Revlon 270 (New York, NY), was applied to all sides except the top surfaces of the enamel blocks before exposure to the demineralization solution. Initially the S and R windows were covered with the acid resistance varnish and the three central windows on both sets of samples were exposed to the same demineralization solution.

Samples were immersed in 40 mL aliquots of the demineralization solution for 48 hours to generate lesions ~ 80–100-μm in depth. The demineralization solution, which was maintained at 37°C and pH 4.8, was composed of 2.0 mmol/L calcium, 2.0 mmol/L phosphate, and 75 mmol/L acetate [28]. After lesions were produced in the central three windows the lesion only windows were covered with acid resistant varnish and then the 4D and 12D windows were exposed to the remineralization solutions continuously for 4 days and 12 days, respectively. The first remineralization model was the neutral remineralization (NR) model that used a supersaturated calcium and phosphate solution with 2 ppm of fluoride at a pH of 7.0. The remineralizing solution was composed of 1.5 mmol/L calcium, 0.9 mmol/L phosphate, 150 mmol/L KCl, and 20 mmol/L HEPES buffer maintained at pH 7.0 and 37°C. To enhance remineralization, 2 ppm fluoride was added to the solution. The second remineralization model, the acidic remineralization (AR) model uses a supersaturated calcium and phosphate solution at a pH of 4.8. The acidic remineralization solution was composed of a 40-mL aliquot of 4.0 mmol/L calcium, 15 mmol/L phosphate, and 50 mmol/L lactic acid and 20 mmol/L HEPES buffer. Fluoride, 20 ppm, was added to enhance remineralization and the samples were incubated at 37°C. The acidic pH remineralization model of Yamazaki and Margolis [38] yields more complete remineralization of the lesions. The lower pH inhibits the rapid formation of a surface zone and allows better mineral deposition in the body of the lesion. Simulated lesions produced using both of these models have been assessed previously using optical coherence tomography [14–17,39]. After exposure of the last treatment windows to 12 days of remineralization the acid resistant varnish was removed from all the windows by rinsing with acetone. Each sample was then stored in a 0.1% thymol solution to prevent fungal and bacterial growth.

2.2 Digital Microscopy

Images of the tooth occlusal surfaces were examined using a digital microscopy/3D surface profilometry system, the VHX-1000 from Keyence (Elmwood, NJ) with the VH-Z25 lens with a polarization attachment for cross polarization reflectance images. A magnification of

25 x was used. Depth composition (DC) images were acquired by scanning the image plane of the microscope and reconstructing a 2D image with all points at optimum focus.

2.3 Optical Coherence Tomography (OCT)

An IVS-2000-HR-C OCT system from Santec (Komaki, Aichi, Japan) was used for this study. This system utilizes a swept laser source and a handpiece with a microelectromechancial (MEMS) scanning mirror and the imaging optics. It is capable of acquiring complete tomographic images of a volume of 5 × 5 × 5mm in approximately 3 seconds. The body of the handpiece is 7 × 18 cm with an imaging tip that is 4 cm long and 1.5 cm across. This system operates at a wavelength of 1312-nm with a bandwidth of 173-nm with a measured resolution in air of 8.8 μm (3 dB). Measured lesion depths were divided by 1.6, the refractive index of enamel. The lateral resolution is 30-μm ($1/e^2$) with a measured imaging depth of 5-mm in air. A thin layer of glycerin was applied to the surface of each bovine enamel block to reduce specular reflection to improve image quality. Image analysis and the measurement of the lesion depth was carried out using Dragonfly from ORS (Montreal, Canada). The lesion depth was measured manually by measuring the depth at the center of each window. The intensity range was adjusted to 20–44 dB for the NR group and 10–44 dB for the AR group to better visualize the lesions as can be seen in Figs. 2 & 3.

2.4 SWIR Dehydration Measurements

Samples were stored in a moist environment to preserve internal hydration and the samples were immersed in the water bath for at least 30 seconds before mounting and performing the dehydration measurements. A computer controlled air nozzle with a 1 mm aperture and an air pressure set to 25 psi was positioned 4 cm away at a 20° angle above from the sample as shown in Fig. 1. After each sample was removed from the water bath, an image was captured as an initial reference image and the pressurized air nozzle was activated to dehydrate the sample. Each measurement consisted of capturing a sequence of images at 10 frames per second for 45 seconds. For each measurement, the air nozzle and the light source were centered on the region of interest (ROI) that encompasses the entire sample. The dehydration setup was completely automated using LabVIEW software (National Instruments, Austin, TX).

A Xenics (Leuven, Belgium) Model Xeva-2.35–320 extended range InGaAs camera sensitive from 900–2350-nm (320×240 pixel) with a Navitar SWIR optimized f=35-mm lens(f/1.4) and a high extinction polarizer was used to acquire images from 1500–2350-nm. The quantum efficiency peaks at 1500-nm near 65% and drops off rapidly to 30% after 1700-nm and drops off again to below 20% after 2000-nm. A Model SLS202 extended wavelength tungsten-halogen light source (Thorlabs, Newton, NJ), from Thorlabs (Newton, NJ) with a peak output at 1500-nm and collimating optics and a high extinction polarizer was used. A polarized, broadband amplified spontaneous emission (ASE) light source Model AP-ASE-2000 from AdValue Photonics (Tucson, AZ) with a center wavelength of 1959-nm and a bandwidth of ~100-nm (−3 dB), 230-nm (−30 dB) and an output power of 11-mW was used as the 1950-nm light source. The light sources were placed at 20° angles to the camera as shown in Fig. 1. Images were processed and automatically analyzed using a dedicated program constructed with LabVIEW software. The intensity change after

dehydration, ΔI, i.e., the intensity difference between the final and initial images, ΔI (t=45), was calculated using $I_{45} - I_0$, where I_{45} is the mean intensity at t = 45 seconds and I_0 is the mean intensity prior to turning on the air nozzle.

In addition the contrast between each treatment window and the sound window was calculated using the following formula: $C_x = (I_x - I_S) / I_x$ where X = L, 4D, 12D, R.

2.5 Polarized Light Microscopy (PLM) and Transverse Microradiography (TMR)

After sample imaging was completed, 200 μm thick serial sections were cut using an Isomet 5000 saw (Buehler, IL) for PLM and TMR. PLM was carried out using a Model RZT microscope from Meiji Techno Co., LTD (Saitama, Japan) with an integrated digital camera, an EOS Digital Rebel XT from Canon Inc. (Tokyo, Japan). The sample sections were imbibed in water and examined in the bright-field mode with crossed polarizers and a red I plate with 500 nm retardation. PLM images were acquired at 7.5x and 15x magnifications.

A custom built TMR system was used to measure the volume percent mineral content in the areas of demineralization on the tooth sections [35]. High-resolution microradiographs were taken using Cu Kα radiation from a Philips 3100 X-ray generator and a Photonics Science FDI X-ray digital imager (Microphonics, Allentown, PA). The X-ray digital imager consisted of a 1392 × 1040 pixel interline CCD directly bonded to a coherent fiber-optic coupler that transfers the light from an optimized gadolinium oxysulfide scintillator to the CCD sensor. The pixel resolution was 2.15 μm and the images were acquired at 10 frames per second. A high-speed motion control system with Newport UTM150 and 850G stages and an ESP300 controller coupled to a video microscopy and a laser targeting system were used for precise positioning of the sample in the field of view of the imaging system. Raw TMR images were converted to volume percent mineral content as described in reference [35].

2.6 Statistical Analysis

ΔI values for the windows of the NR and AR sets for each wavelength were compared using one-way analysis of variance with repeated measures (RM-ANOVA) with Tukey's multiple comparisons post-test. In addition, the ΔI values at each wavelength 1500–2340 vs 1950-nm were compared for each treatment window using a two-tailed paired t-test. Prism 7 statistical software (GraphPad Software, Inc., La Jolla, CA) was used for the calculations. Significance level was set at $p < 0.05$.

RESULTS

3.1 Simulated Lesion Models

Digital light microscope images of bovine blocks from each of the lesion models are shown in Figs. 2A and 3A. Areas of demineralization appear whiter in the images. Such areas are clearly visible in the L, 4D and 12D windows of Fig. 2A for the neutral remineralization (NR) model. The lesion only appears intact near the center of the L window and erosion is visible at the top and bottom of the window. The 4D and 12D windows appear more uniform and intact. Erosion was present in the L window for 6 out of the 10 samples for

the NR model. Since erosion was not observed for the other treatment windows it is likely the erosion/damage occurred when the windows were rinsed with acetone to remove the acid resistant varnish. The border of the laser cut incision at the border of each window have enhanced resistance to acid dissolution and typically remain intact. These marks can be used to determine the amount of the lesion in the L window that have been lost to erosion and this loss was corrected for the L window. Extra bovine blocks were also produced using each model for PLM and TMR analysis and they were sectioned to produce 200-μm thick sections. Fig. 2B shows the PLM image of a slice. Areas of demineralization appear black and lesion areas are clearly visible in the L, 4D and 12 D windows. The L window shows some erosion and the demineralization appears thinner than for the other two windows that have intact surfaces. A TMR image is shown in Fig. 2C, and the lesions are visible in the 4D and 12D windows and the mineral loss in the lesion body is 10–15%. A surface zone of higher mineral content is visible in the 12D window showing 80% by volume mineral or a mineral loss of 5%. OCT scans are shown for another sample from this group in Figs. 2D & 2E, two images of the same slice or b-scan are shown with two different intensity ranges, the full intensity range 0–60 dB and a narrowed range of 10 to 44 dB that better highlights areas of demineralization. Demineralized areas are clearly visible in the L, 4D and 12D windows. The mean lesion depth was measured for all the samples and the mean lesion depth was between 80 and 100-μm. Close inspection of the 12D window shows a dark band midway through the lesion, this indicates that a transparent surface zone is present on this lesion window. For this model five of the samples had a transparent surface zone visible for the 12D windows with a mean (SD) thickness of 38.8 (4.55) μm and one of the 4D windows had a transparent surface zone of 44 μm.

Digital light microscope images for the acidic remineralization (AR) model are shown in Fig. 3A and they appear similar in nature to those for the NR model. In this case all the windows appear uniform and intact. The 4D and 12D windows shown in Fig. 3B for a sample exposed to the AR model are very different to those shown in Fig. 2B. Instead of a single layer of demineralization as was observed for the NR model three distinct layers were observed, a dark layer of demineralization ~ 80–100-μm thick followed by a layer of transparent enamel ~ 50 μm thick followed by another layer of more diffuse lighter demineralization ~ 70 μm thick. Careful inspection of the laser incisions on both sides of the 4D window in Fig. 3B show that the subsurface transparent zone follows the incision boundaries. Since the transparent zones around the incision must have formed during remineralization, this suggests that the underlying transparent zone was formed during exposure to the remineralization solution and is not sound enamel. A TMR image is shown in Fig. 3C, unfortunately none of the structure visible in the PLM images is visible in the TMR images which confirms that the mineral loss in these areas is likely very small. The mean thickness of each layer is listed in Table I. This complex lesion structure was observed for almost all the samples in this group, nine out of ten. The other sample had a structure similar in appearance to the NR model. The L window appeared similar to the NR model group and erosion also occurred for some of the L window samples. The same pattern of demineralization was observed in the OCT images shown in Figs. 3D and 3E. A surface zone was also observed in the outer layer of demineralization for a few of the samples in this group, three of the samples showed a surface zone in both the 4D and 12D windows and

the mean (SD) surface zone thickness was 30 (0) μm and 34.7 (8.08) for the 4D and 12D windows respectively.

3.2 Dehydration Measurements

Images of samples of the NR and AR groups at three time points before (0) at 45 seconds during forced air drying and after drying for a full day (D) are shown for the 1950-nm light source in Fig. 4. The S and R windows are completely dark with intensity values near zero. All the windows have intensity values near zero before drying at time 0. A drying time of 45 seconds was sufficient to produce large changes in intensity in the lesion areas. Further drying for a full day to remove any mobile water in the samples only slightly increased the intensity in those areas although the increase appears to be greater in the 4D and 12D windows.

Profiles of the intensity versus time during 45 seconds of forced air drying for each window are shown for samples of the NR and AR groups at 1950-nm in Fig. 5. There is little change in the intensity for the S and R windows. The L window shows rapid change with a “bump” in the curve when it peaks before leveling off. This bump has been observed in previous studies for the lesion windows and we suspect this bump is due to the presence and removal of pooled water from the surface [22]. Water pools in the rough and highly porous surface. Similar “bumps” in the curves were observed for a few of the 4D and 12D curves but all of the L windows exhibit that behavior. The change in intensity was expected to be less for the 4D and 12D curves for which substantial remineralization has occurred, however, for both the NR and AR groups the intensity rise was instead similar for both the L and 4D curves. We believe the similarity between the L and 4D curves is due to the loss of some of the lesion in the L windows due to erosion during removal of the acid resistant varnish. The 12D curves for both models show a marked reduction in the change in ΔI and some of the curves show a slower change in intensity during drying similar to the 12D curve shown in Fig. 5A. The mean (SD) ΔI values for both models and both wavelengths are listed in Table I. The mean (SD) ΔI values are also plotted in Fig. 6 for both models and both wavelengths. The 1950-nm wavelength yielded significantly higher ($P > 0.05$) ΔI values for most of the treatment windows compared to the 1500–2340-nm wavelength range. There was also a marked and significant reduction in the mean (SD) ΔI values between the L, 4D and the 12D windows for each remineralization model indicating that significant remineralization had occurred.

3.3 Lesion Contrast

The contrast between the sound and treatment groups was calculated for both models and both wavelength ranges for the samples after 45 seconds of forced air drying. The values are tabulated in Table I. Both wavelength ranges yielded extremely high contrast values for the L, 4D and 12D treatment windows for both models. Four of the windows had contrast values of 0.99 for the 1950-nm wavelength.

DISCUSSION

In this study we investigated the contrast of simulated lesions in enamel at longer SWIR wavelengths from 1500–2340-nm and at 1950-nm coincident with the strong water absorption band. The lesion contrast depends on the mineral gradients in the lesion. For example, an active lesion has a higher contrast than an arrested lesion that has a well-defined surface zone of higher mineral content and has a very different distribution of the mineral loss. Therefore, two different models of remineralization were investigated in this study. In addition, we measured the change in intensity of simulated lesions before and after remineralization at these longer wavelengths.

We have previously investigated the contrast of caries lesions at wavelengths longer than 1700-nm and those studies have indicated that the contrast of demineralization on enamel is higher, however there were significant challenges with those studies due to problems acquiring broadband light sources of sufficient intensity at 1950-nm [29]. In a previous study a narrow band 1950-nm fiber laser was used to scan over the tooth surface, however the image quality was poor, high quality polarizers were not used and there was much interference from specular reflection [27]. In that study, simulated lesions of similar severity (~ 100-μm deep) were measured on human tooth occlusal surfaces and the mean (SD) contrast was significantly higher ($p < 0.05$) at 1950 nm (0.80 (0.07)), than for shorter wavelengths. The contrast was also measured at the shorter wavelength and weaker water absorption band at 1468 nm using a broadband ASE light source. The mean (SD) contrast was markedly lower 0.33 (0.13) than at 1950-nm. In this study, a polarized broadband source at 1950-nm was used along with a high extinction SWIR polarizer and there was minimal interference from specular reflection as can be clearly seen in Fig. 4. The contrast of the demineralization in this study, even in those areas where the mineral gradients are greatly reduced was extremely high approaching 0.99 which is much higher than the 0.80 contrast of the previous study using a scanned laser source. The very high contrast is likely due to a combination of the low scattering at 1950-nm and the high water absorption at 1950-nm. At wavelengths of high water absorption, deeply penetrating photons in sound areas are absorbed by the water minimizing backscattered light. Reflection at the enamel surface is suppressed by the cross polarizers.

The main objective of this study was to assess the performance of SWIR dehydration measurements at the strong water absorption band of 1950-nm. In prior studies filtered tungsten-halogen light sources did not have sufficient intensity at 1950-nm to perform these measurements and scanned narrow band lasers are poorly suited for the time-resolved measurements. The high power, polarized, broadband 1950-nm source was ideally suited for these measurements. We observed very large changes in intensity (ΔI) after drying for 45 seconds at 1950-nm and these changes were significantly higher than ΔI for the wavelength range from 1500–2340-nm, suggesting that the 1950-nm wavelength band is advantageous for dehydration measurements on tooth coronal surfaces to assess lesion activity. Both wavelength regions were also able to measure a significant decrease in ΔI on windows where increased remineralization has occurred, i.e., lesion areas that have become more arrested. A significant concern regarding the high magnitude of the water absorption band at 1950-nm was that any residual water would greatly lower contrast and

that it would be difficult to sufficiently dehydrate the lesions in a reasonable period of time. However, 45 seconds of dehydration was sufficient to produce large changes in intensity and a comparison with the fully desiccated samples (24-hrs) in Fig. 4 suggest a dehydration time of 45 seconds is sufficient. The intensity in lesion areas is noticeably higher after 24-hrs however the difference is not sufficiently large to suggest that much longer dehydration times are necessary. Higher air pressures can also be investigated to accelerate dehydration. The air pressure for dehydration was set at 25 psi which is fairly low compared to the 50–80 psi air pressures typically set for the dental air-water syringe.

It is interesting to compare the performance of OCT and SWIR imaging for assessing remineralization on these samples. Remineralization can be detected with OCT by the development of a transparent surface zone on the surface, however in this study many of the remineralization windows did not manifest measurable transparent surface zones. It is likely that the lesions underwent significant remineralization, however the mineral content did not increase sufficiently to appear transparent in the OCT images. The acidic remineralization windows produced many lesions with large transparent zones deeper in the lesions with increased remineralization of the lesion body. The unusual structure present in the 4D and 12D windows for the AR model was most likely caused by increased demineralization below the surface and an increase in the lesion depth as has been observed previously with this model [22]. SWIR imaging at both wavelength ranges was able to detect large changes in ΔI with increasing remineralization. The results are somewhat complicated by erosion in the lesion only windows which likely reduced the expected mean ΔI values as the lesion windows were expected to have higher ΔI values than the 4D windows. However, large differences were observed between the 4D and 12D windows for both models which were not contaminated by erosion.

In summary, this study shows that imaging at 1950-nm near the strong water absorption band yields the highest contrast of demineralization on tooth surfaces. Therefore, this wavelength is best suited for imaging caries lesions on tooth surfaces in reflectance. In addition, the contrast of that demineralization increases markedly at 1950-nm after drying tooth surfaces for several seconds indicating this wavelength is ideally suited for use for the assessment of lesion activity by SWIR imaging during dehydration. This can be accomplished clinically by using an SWIR imaging handpiece with an integrated air nozzle [40]. The next step is to image caries lesions on tooth coronal surfaces *in vivo* after nonsurgical intervention with fluoride to show that SWIR imaging can be used to monitor changes in lesion activity and such studies are currently underway at UCSF.

Supplementary Material

Refer to Web version on PubMed Central for supplementary material.

ACKNOWLEDGEMENTS

This work was supported by NIH/NIDCR grants R01-DE027335 and R01-DE028295 and Swiss National Science Foundation (SNSF) grant P2GEP3-188157. The authors would also like to acknowledge the contributions of Nick Chang, Jacob Simon, and Yihua Zhu.

REFERENCES

1. Fejerskov O, Nyvad B, Kidd E, editors. Dental Caries: The Disease and its Clinical Management: Wiley Blackwell. 2015.
2. Ekstrand KR, Zero DT, Martignon S, Pitts NB. Lesion activity assessment. Monographs in Oral Science2009; 21:63–90. [PubMed: 19494676]
3. Ismail AI, Sohn W, Tellez M, Amaya A, Sen A, Hasson H, Pitts NB. The International Caries Detection and Assessment System (ICDAS): an integrated system for measuring dental caries. Community Dent Oral Epidemiol2007; 35(3):170–178. [PubMed: 17518963]
4. Pitts N"ICDAS"--an international system for caries detection and assessment being developed to facilitate caries epidemiology, research and appropriate clinical management. Community Dent Health2004; 21(3):193–198. [PubMed: 15470828]
5. Pitts N, editor. Detection, Assessment, Diagnosis and Monitoring of Caries. Volume 21. Basel: Karger. 2009.
6. Kidd EA. The histopathology of enamel caries in young and old permanent teeth. British dental journal1983; 155(6):196–198. [PubMed: 6578821]
7. Kidd E, Fejerskov O. What Constitutes Dental Caries ? Histopathology of carious enamel and dentin related to the action of cariogenic biofilms. J Dent Res2004; 83(C):C35–C38. [PubMed: 15286119]
8. Artun J, Thylstrup A. A 3-year clinical and SEM study of surface changes of carious enamel lesions after inactivation. Am, J Orthod Dentofac Orthop1989; 95(4):327–333.
9. Silverstone LM. Remineralizing phenomena. Caries Res1977; 11(1):59–84. [PubMed: 318574]
10. Bergstrom DH, Fox JL, Higuchi WI. Quantitative microradiography for studying dental enamel demineralization and remineralization. J Pharm Sci1984; 73(5):650–653. [PubMed: 6737239]
11. Wefel JS, Harless JD. Comparison of artificial white spots by microradiography and polarized light microscopy. J Dent Res1984; 63(11):1271–1275. [PubMed: 6094633]
12. Arends J, Ruben JL, Inaba D. Major topics in quantitative microradiography of enamel and dentin: R parameter, mineral distribution visualization, and hyper-remineralization. Adv Dent Res1997; 11(4):403–414. [PubMed: 9470497]
13. Chan KH, Tom H, Lee RC, Kang H, Simon JC, Staninec M, Darling CL, Pelzner RB, Fried D. Clinical monitoring of smooth surface enamel lesions using CP-OCT during nonsurgical intervention. Lasers Surg Med2016; 48(10):915–923. [PubMed: 26955902]
14. Jones RS, Darling CL, Featherstone JD, Fried D. Remineralization of in vitro dental caries assessed with polarization-sensitive optical coherence tomography. J Biomed Opt2006; 11(1):014016. [PubMed: 16526893]
15. Jones RS, Fried D. Remineralization of enamel caries can decrease optical reflectivity. J Dent Res2006; 85(9):804–808. [PubMed: 16931861]
16. Kang H, Darling CL, Fried D. Nondestructive monitoring of the repair of enamel artificial lesions by an acidic remineralization model using polarization-sensitive optical coherence tomography. Dent Mater2012; 28(5):488–494. [PubMed: 22204914]
17. Lee RC, Kang H, Darling CL, Fried D. Automated assessment of the remineralization of artificial enamel lesions with polarization-sensitive optical coherence tomography. Biomed Opt Express2014; 5(9):2950–2962. [PubMed: 25401009]
18. Stookey GK. Quantitative light fluorescence: a technology for early monitoring of the caries process. Dent Clin North Am2005; 49(4):753–770, vi. [PubMed: 16150315]
19. Ando M, Stookey GK, Zero DT. Ability of quantitative light-induced fluorescence (QLF) to assess the activity of white spot lesions during dehydration. Am J Dent2006; 19(1):15–18. [PubMed: 16555651]
20. Ando M, Ferreira-Zandona AG, Eckert GJ, Zero DT, Stookey GK. Pilot clinical study to assess caries lesion activity using quantitative light-induced fluorescence during dehydration. J Biomed Opt2017; 22(3):35005. [PubMed: 28280839]
21. Lee C, Lee D, Darling CL, Fried D. Nondestructive assessment of the severity of occlusal caries lesions with near-infrared imaging at 1310 nm. J Biomed Opt2010; 15(4):047011. [PubMed: 20799842]

22. Lee RC, Darling CL, Fried D. Assessment of remineralization via measurement of dehydration rates with thermal and near-IR reflectance imaging. J Dent2015; 43:1032–1042. [PubMed: 25862275]
23. Lee RC, Darling CL, Fried D. Assessment of remineralized dentin lesions with thermal and near-infrared reflectance imaging. In: Laser in Dentistry XXII; 2016. Proc. SPIE Vol. 96920 0B:1–5.
24. Yang V, Zhu Y, Curtis D, Le O, Chang N, Fried W, Simon JC, Banan P, Darling C, Fried D. Thermal imaging of root caries in vivo. J Dent Res2020; 99(13):1502–1508. [PubMed: 32866422]
25. Chang NN, Jew JM, Fried D. Lesion dehydration rate changes with the surface layer thickness during enamel remineralization. In: Lasers in Dentistry XXIV; 2018. Proc. SPIE Vol. 10473 0D:1–7.
26. Darling CL, Huynh GD, Fried D. Light Scattering Properties of Natural and Artificially Demineralized Dental Enamel at 1310-nm. J Biomed Optics2006; 11(3):034023
27. Chan KH, Fried D. Multispectral cross-polarization reflectance measurements suggest high contrast of demineralization on tooth surfaces at wavelengths beyond 1300-nm due to reduced light scattering in sound enamel. J Biomed Opt2018; 23(6):060501.
28. Chung S, Fried D, Staninec M, Darling CL. Multispectral near-IR reflectance and transillumination imaging of teeth Biomed Opt Express2011; 2(10):2804–2814. [PubMed: 22025986]
29. Ng C, Almaz EC, Simon JC, Fried D, Darling CL. Near-infrared imaging of demineralization on the occlusal surfaces of teeth without the interference of stains. J Biomed Optics2019; 24(3):036002.
30. Fried WA, Chan KH, Fried D, Darling CL. High Contrast Reflectance Imaging of Simulated Lesions on tooth occlusal surfaces at near-IR wavelengths. Lasers Surg Med2013; 45(8):533–541. [PubMed: 23857066]
31. Simon JC, Chan KH, Darling CL, Fried D. Multispectral near-IR reflectance imaging of simulated early occlusal lesions: variation of lesion contrast with lesion depth and severity. Lasers Surg Med2014; 46(3):203–215. [PubMed: 24375543]
32. Simon JC, Lucas SA, Lee RC, Staninec M, Tom H, Chan KH, Darling CL, Fried D. Near-IR transillumination and reflectance imaging at 1300-nm and 1500–1700-nm for in vivo caries detection. Lasers Surg Med2016; 48(6):828–836. [PubMed: 27389018]
33. Wu J, Fried D. High contrast near-infrared polarized reflectance images of demineralization on tooth buccal and occlusal surfaces at lambda = 1310-nm. Lasers Surg Med2009; 41(3):208–213. [PubMed: 19291753]
34. Zakian C, Pretty I, Ellwood R. Near-infrared hyperspectral imaging of teeth for dental caries detection. J Biomed Optics2009; 14(6): 064047.
35. Darling CLD, Featherstone JDB, Le CQ, Fried D, "An automated digital microradiography system for assessing tooth demineralization," In: Lasers in Dentistry VX; 2009 Proc. SPIE Vol. 7162, 1–7.
36. Mellberg JR. Hard-tissue substrates for evaluation of cariogenic and anti-cariogenic activity in situ. J Dent Res1992; 71Spec No:913–919. [PubMed: 1592986]
37. Yamazaki H, Litman A, Margolis HC. Effect of fluoride on artificial caries lesion progression and repair in human enamel: regulation of mineral deposition and dissolution under in vivo-like conditions. Arch Oral Biol2007; 52(2):110–120. [PubMed: 17049334]
38. Yamazaki H, Margolis HC. Enhanced enamel remineralization under acidic conditions in vitro. J Dent Res2008; 87(6):569–574. [PubMed: 18502967]
39. Kang H, Jiao JJ, Chulsung L, Le MH, Darling CL, Fried DL. Nondestructive assessment of early tooth demineralization using cross-polarization optical coherence tomography. Sel Top Quant Elect, IEEE J2010; 16(4):870–876.
40. Chang NN, Zhu Y, Curtis DA, Le O, Yang V, Fried WA, Simon J, Banan P, Darling CL, Fried D. SWIR, thermal and CP-OCT imaging probes for the *in vivo* assessment of the activity of root caries lesions. In: Lasers in Dentistry XXVI; 2020. Proc. SPIE Vol. 11217 08:1–6.

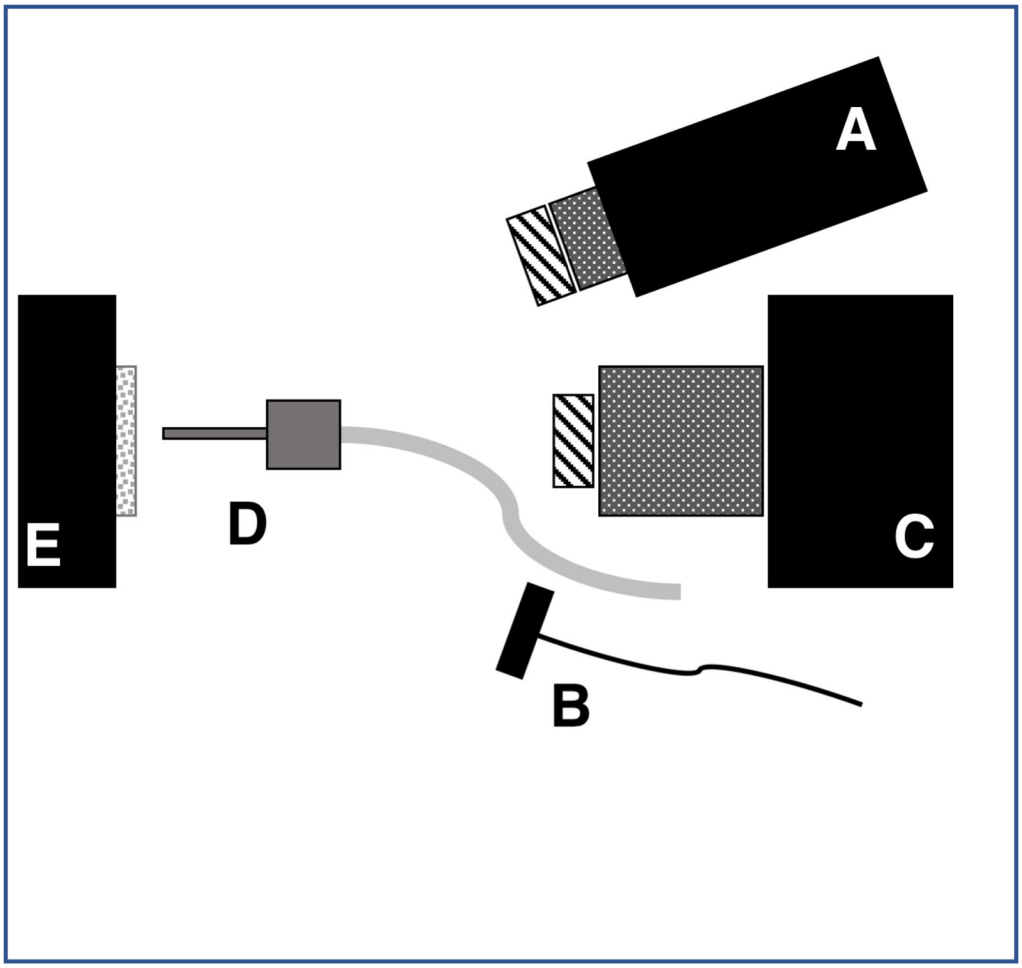

Figure 1.
Schematic of the experimental setup showing (A) tungsten-halogen light source with 1500-nm longpass filter, collimating lens and polarizer, (B) polarized 1950-nm fiber optic light source, (C) Xenics extended range InGaAs camera with lens and polarizer, (D) air nozzle and (E) bovine tooth samples mounted on XYZ stage.

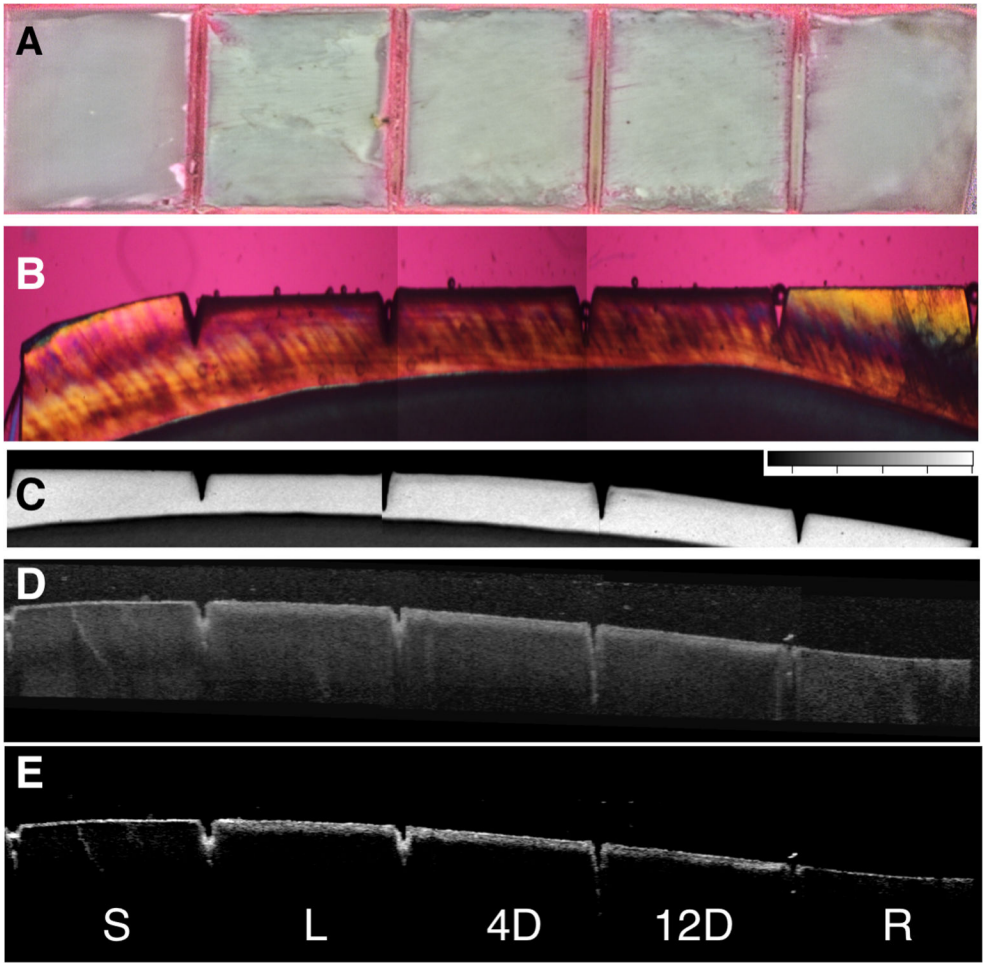

Figure 2.

(A) Digital microscopy image of one of the bovine blocks produced using the neutral remineralization model (NR) showing the five windows, (B) PLM and (C) TMR images of a 200-μm thick slice cut from one of samples, and raw − 0 – 70 dB (D) and reduced intensity range − 20–44 dB (E) OCT b-scans from one of the samples.

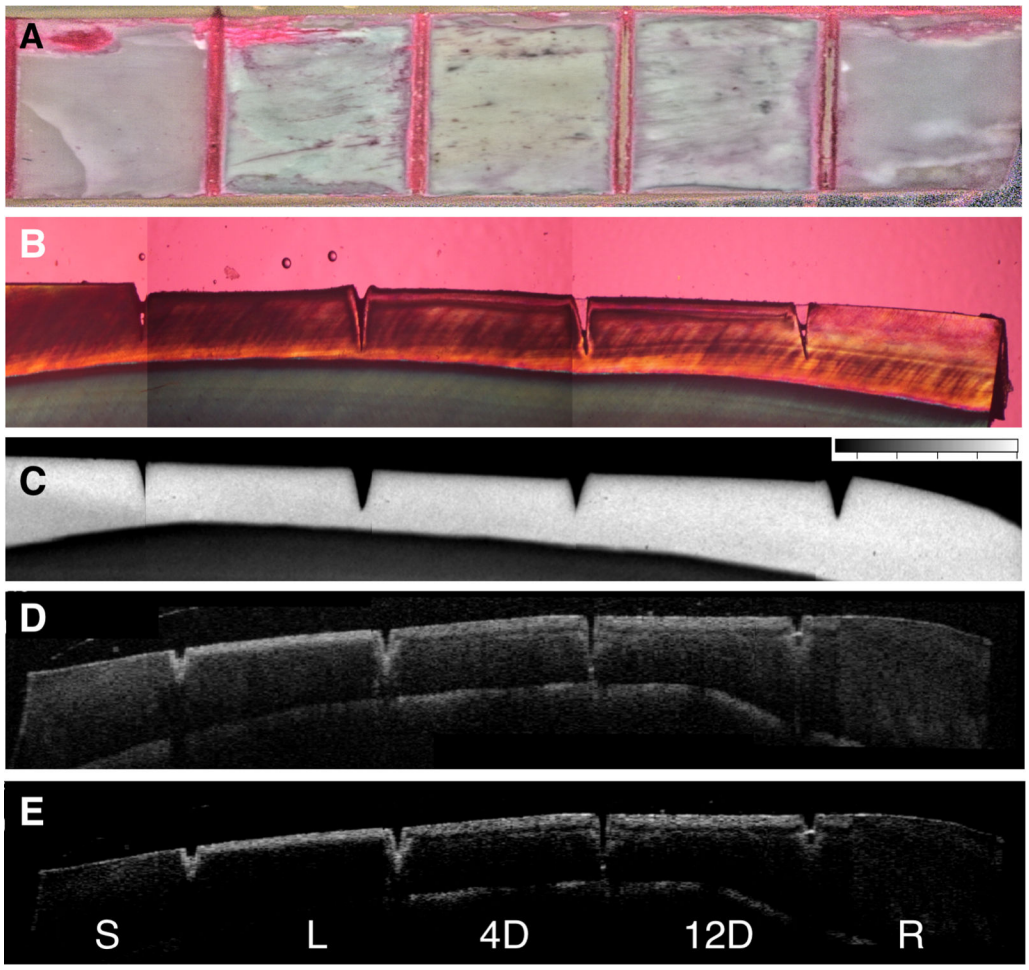

Figure 3.

(A) Digital microscopy image of one of the bovine blocks produced using the acidic remineralization model (AR) showing the five windows, (B) PLM and (C) TMR images of a 200-μm thick slice cut from one of samples, and raw − 0 – 70 dB (D) and reduced intensity range − 10–44 dB (E) OCT b-scans of one of the samples.

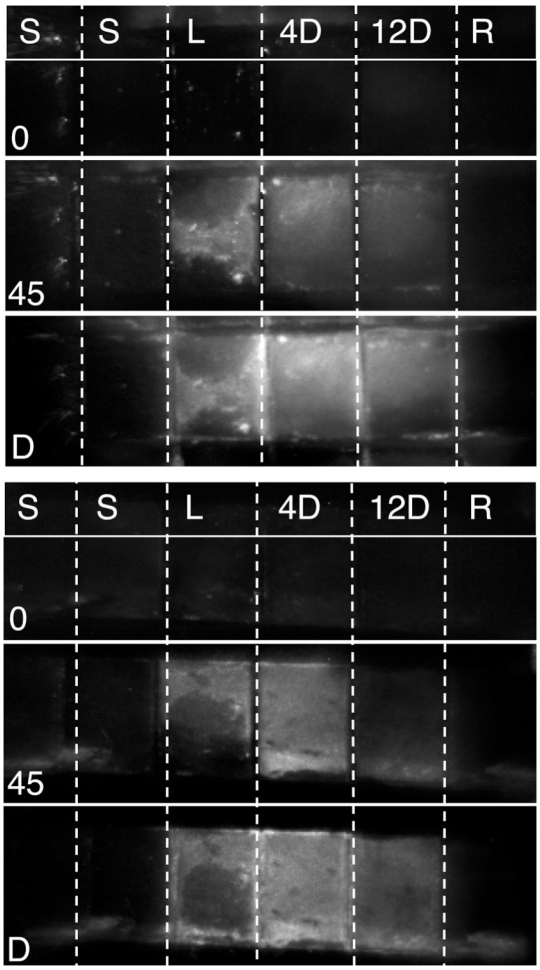

Figure 4.

Images of samples from the Neutral (top) and Acidic (bottom) remineralization models taken at 1950-nm before, after drying for 45 seconds and after 1-Day (D) of drying. The vertical dashed lines separate each of the labeled windows on the bovine blocks. At time zero all the windows are almost completely black.

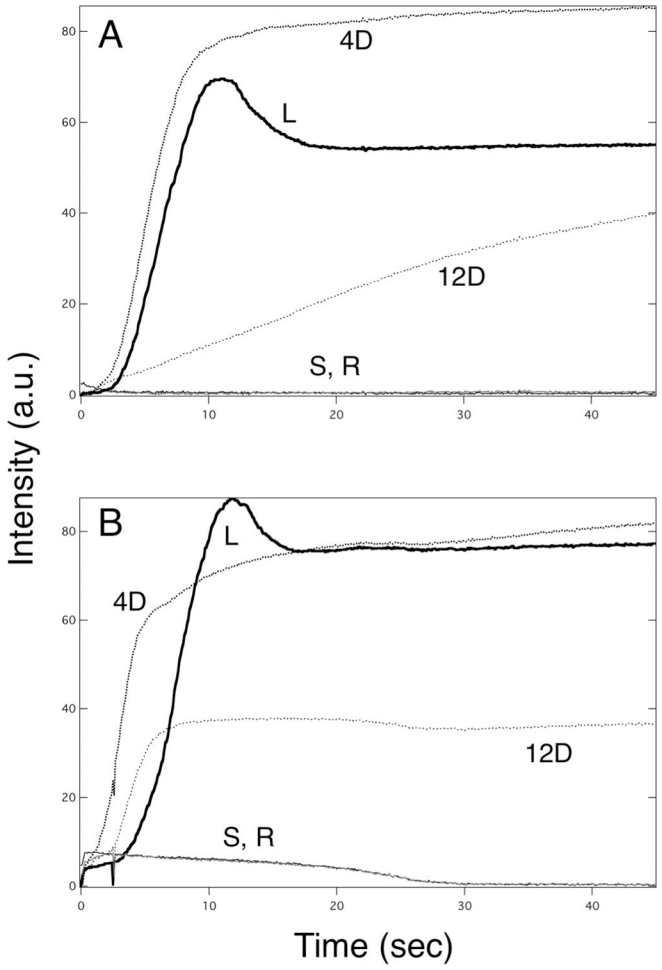

Figure 5.

Intensity profiles for the five windows, sound-thin solid black line, lesion - thick solid black line, 4-day remin-thick dotted black line, lesion- thin dotted black line, and remin control – thin gray line. (A) Neutral and (B) Acidic remineralization models recorded at 1950-nm for one of the samples from each group, respectively.

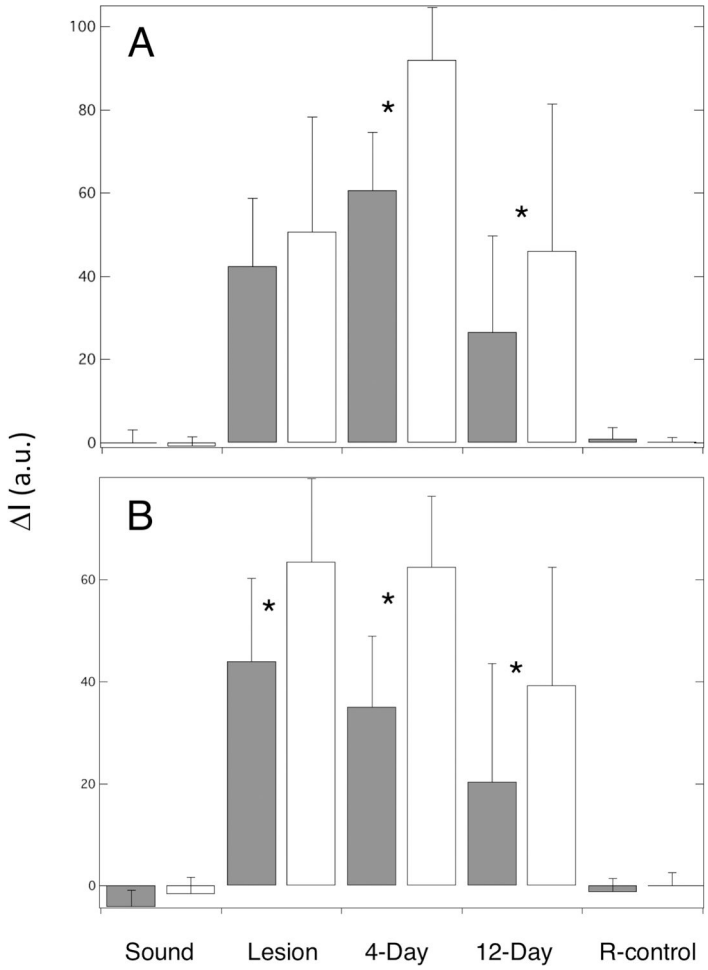

Figure 6.

Plots of the mean (SD) ΔI for the (A) Neutral and (B) Acidic remineralization models at 1500–2340-nm (black bars) and 1950-nm (white bars). Asterisks indicate that ΔI was significantly different ($P < 0.05$) between each wavelength for that window.

Table I.

The mean (SD) of the lesion depths (LD) measured with OCT for the windows of the neutral (NR) and the acidic remineralization (AR) models. Note each depth has been divided by 1.6 to account for the refractive index of enamel. For the AR windows the distance to the base of the 1st layer of demineralization, the base of the intermediate transparent zone and the base of the 2nd layer of demineralization are indicated if present. The mean (SD) values for ΔI and the contrast between the sound and other windows from SWIR imaging are also listed for both models and wavelengths. For, ΔI, groups across each row with the same letter are not significantly different, p >0.05.

	Sound	**Lesion**	**4-Day**	**12-Day**	**Remin Ctrl**
OCT					
Mean LD, μm (NR)	-	92.7(12.1)	83.7(16.1)	81.3(13.4)	-
Mean LD, μm (AR)	-	98.3(15.2)	87.6(12.5) 133(20.1) 200(40.2)	84.2(14.4) 130(15.8) 207(37.1)	-
SWIR Imaging					
Mean ΔI (NR)					
1950-nm	0.72(0.84)	51.7(27.4) a,b	92.7(14.2)b	47.1(36.9) a	0.90(0.75)
1500-nm	1.76(1.32)	42.8(16.7) a,b	61.2(13.9)b	27.4(23.1) a	2.33(2.09)
Mean ΔI (AR)					
1950-nm	0.34(0.15)	64.0(25.5) a	62.9(23.2) a	39.9(24.6) b	2.06(2.49)
1500-nm	2.07(1.74)	48.5(13.2) a	39.4(12.3) a	21.3(10.1) b	1.68(2.16)
Mean Contrast (NR)					
1950-nm	0	0.98(0.04)	0.99(0.01)	0.95(0.09)	0.13(0.44)
1500-nm	0	0.95(0.05)	0.97(0.02)	0.80(0.25)	− 0.99(2.8)
Mean Contrast (AR)					
1950-nm	0	0.99(0.0)	0.99(0.0)	0.99(0.01)	0.56(0.39)
1500-nm	0	0.96(0.04)	0.95(0.04)	0.90(0.07)	− 0.97(1.7)